CHALMERS
UNIVERSITY OF TECHNOLOGY

Unsupervised Learning for Gain-Phase Impairment Calibration in ISAC Systems

Citation for the original published paper (version of record):
Mateos Ramos, J., Häger, C., Keskin, M. et al (2025). Unsupervised Learning for Gain-Phase Impairment Calibration in ISAC Systems. ICASSP, IEEE International Conference on Acoustics, Speech and Signal Processing - Proceedings.
http://dx.doi.org/10.1109/ICASSP49660.2025.10890700

(article starts on next page)

Unsupervised Learning for Gain-Phase Impairment Calibration in ISAC Systems

José Miguel Mateos-Ramos*, Christian Häger*, Musa Furkan Keskin*,
Luc Le Magoarou†, Henk Wymeersch*
*Department of Electrical Engineering, Chalmers University of Technology, Sweden
†Univ Rennes, INSA Rennes, CNRS, IETR-UMR 6164, Rennes, France

***Abstract*—Gain-phase impairments (GPIs) affect both communication and sensing in 6G integrated sensing and communication (ISAC). We study the effect of GPIs in a single-input, multiple-output orthogonal frequency-division multiplexing ISAC system and develop a model-based unsupervised learning approach to simultaneously (i) estimate the gain-phase errors and (ii) localize sensing targets. The proposed method is based on the optimal maximum a-posteriori ratio test for a single target. Results show that the proposed approach can effectively estimate the gain-phase errors and yield similar position estimation performance as the case when the impairments are fully known.**

***Index Terms*—GPIs, Orthogonal frequency-division multiplexing, Model-based learning, Unsupervised learning.**

I. Introduction

Integrated sensing and communication (ISAC) is considered a key enabler of the 6th generation wireless systems (6G) [1], combining sensing and communication functions in a single device, thereby providing sensing capabilities to communication systems, while also improving wireless channel usage efficiency and system performance [2]. Signal processing in ISAC has been largely driven by model-based algorithms, which offer performance guarantees, explainability, and predictable computational complexity [3]–[7]. However, the higher carrier frequencies expected in 6G and the integration of sensing in communication networks increase the likelihood of hardware impairments such as antenna distortions, phase noise, and sampling jitter [8], [9]. These hardware impairments cause a model mismatch in the model-based algorithms and thus degrade their performance.

Deep learning (DL) has been successfully applied to mitigate hardware impairments in ISAC [10]–[13], but it suffers from lack of interpretability. In contrast, model-based machine learning (MB-ML) provides interpretable solutions, by parameterizing standard model-based algorithms, enhancing their adaptability to mismatched models while offering performance guarantees [14]. MB-ML has been applied in communications [15]–[18], sensing [19]–[21], and ISAC scenarios [22]. Hardware impairment mitigation solutions (e.g., [20]–[22]) rely on supervised learning (SL), which involves the difficult or time-consuming process of acquiring the ground-truth position of the objects in the environment. Unsupervised learning (UL) avoids labeled data and has been applied for ISAC inter-antenna spacing impairment mitigation in [23], though still requiring a small labeled dataset to fully compensate for the impairments.

This work was supported, in part, by a grant from the Chalmers AI Research Center Consortium (CHAIR), by the National Academic Infrastructure for Supercomputing in Sweden (NAISS), the Swedish Foundation for Strategic Research (SSF) (grant FUS21-0004, SAICOM), Hexa-X-II, part of the European Union's Horizon Europe research and innovation programme under Grant Agreement No 101095759, and Swedish Research Council (VR grant 2022-03007). The work of C. Häger was also supported by the Swedish Research Council under grant no. 2020-04718. The work of L. Le Magoarou is supported by the French national research agency (grant ANR-23-CE25-0013)

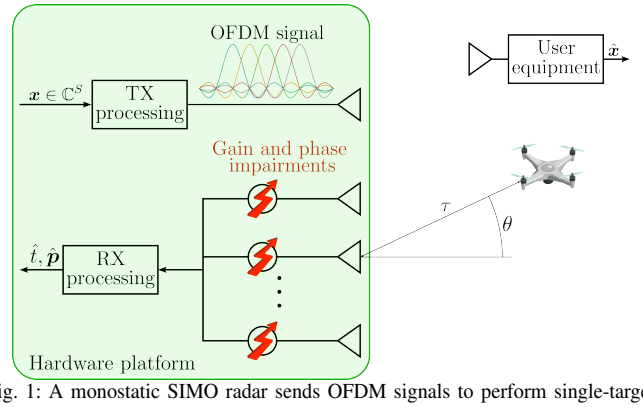

Fig. 1: A monostatic SIMO radar sends OFDM signals to perform single-target detection and position estimation. The OFDM signals can be received by a user equipment to estimate the transmitted messages and reflected back from a target in the environment. The receive antenna array is affected by GPIs.

In this paper, we develop an UL approach to jointly compensate for antenna gain-phase impairments (GPIs) and estimate target locations, under the MB-ML framework. As a proof-of-concept, we focus on a simple monostatic single-input multiple-output (SIMO) radar performing single-target detection and position estimation based on orthogonal frequency-division multiplexing (OFDM) signals (see Fig. 1). GPI mitigation is an important problem, with model-based [24]–[26], DL [27], [28], and MB-ML solutions [17], [18]. However, [24], [25] required at least a transmitter at a known angle to calibrate the antenna array and [26] assumed a known model of the channel state information (CSI), which does not apply to our case as the CSI contains the target position to be estimated. In [27], only angle estimation was performed and [28] required a transmitter at a known position for calibration. Moreover, [27], [28] require labeled data to train. Finally, although [17], [18] proposed MB-ML UL approaches to compensate for GPI, they considered a pure communication system and CSI estimation without localization of the user.

II. System Model

We consider a monostatic SIMO-OFDM ISAC transceiver equipped with a single-antenna transmit (TX) and a receive

(RX) uniform linear array (ULA) of N elements. The element spacing of the RX ULA is d_{R}. The OFDM signal has a symbol duration of $T_{\mathrm{sym}} = T_{\mathrm{cp}} + T$, where T_{cp} is the cyclic prefix (CP) and and T is the elementary symbol duration. The complex baseband OFDM transmit signal with S subcarriers and a subcarrier spacing $\Delta_{\mathrm{f}} = 1/T$ is [29], [30]

$$s(t) = \frac{1}{\sqrt{S}} \sum_{s=0}^{S-1} x_s e^{\jmath 2\pi s \Delta_{\mathrm{f}} t} \mathrm{rect}\left(\frac{t}{T_{\mathrm{sym}}}\right), \tag{1}$$

where x_s is the complex transmitted symbol in the s-th subcarrier. Considering the presence of a stationary point-target in the far-field, the noise-free received baseband signal at the n-th RX element is [31]

$$z_n(t) = \gamma [\boldsymbol{a}(\theta)]_n s(t - \tau) \tag{2}$$

where γ is the complex channel gain, τ is the total round-trip delay of the target, θ is the angle-of-arrival (AOA), and $\boldsymbol{a}(\theta)$ is the array steering vector with

$$[\boldsymbol{a}(\theta)]_n = e^{-\jmath 2\pi n d_{\mathrm{R}} \sin(\theta)/\lambda}, n = 0, \ldots, N-1 \tag{3}$$

for carrier wavelength λ. Following the standard OFDM assumption, the CP is taken to be larger than the round-trip delay of the furthermost target, i.e., $T_{\mathrm{cp}} \geq \tau$. Sampling $z_n(t)$ at $t = T_{\mathrm{cp}} + lT/S$ for $l = 0, \ldots, S-1$ (i.e., after CP removal), we obtain the discrete-time signal

$$z_n[l] = \frac{\gamma}{\sqrt{S}} [\boldsymbol{a}(\theta)]_n \sum_{s=0}^{S-1} x_s e^{\jmath 2\pi s \frac{l}{S}} e^{-\jmath 2\pi s \Delta_{\mathrm{f}} \tau}, \tag{4}$$

where the known phase shift $\exp(\jmath 2\pi s \Delta_{\mathrm{f}} T_{\mathrm{cp}})$ is absorbed into x_s. Taking the S-point DFT of $z_n[l]$ yields the frequency-domain baseband signal as

$$Z_{n,s} = \mathcal{F}\big\{\{z_n[l]\}_{l=0}^{S-1}\big\} = \gamma [\boldsymbol{a}(\theta)]_n x_s [\boldsymbol{b}(\tau)]_s, \tag{5}$$

with $[\boldsymbol{b}(\tau)]_s = \exp(-\jmath 2\pi s \Delta_{\mathrm{f}} \tau)$. Aggregating over antenna elements and subcarriers, the signal in (4) can be expressed as

$$\boldsymbol{Z} = \gamma \boldsymbol{a}(\theta)(\boldsymbol{b}(\tau) \odot \boldsymbol{x})^{\top} \in \mathbb{C}^{N \times S}, \tag{6}$$

where $\boldsymbol{x} = [x_0 \cdots x_{S-1}]^{\top}$ is the transmit symbol vector and $\odot$ denotes the Hadamard product.

Observation without GPI: Adding noise at the receiver side and considering the random presence of a target in the environment yields the final model[1]

$$\boldsymbol{Y} = t\gamma \boldsymbol{a}(\theta)(\boldsymbol{b}(\tau) \odot \boldsymbol{x})^{\top} + \boldsymbol{W}, \tag{7}$$

where $t \in \{0, 1\}$ denotes the absence or presence of a target and $\boldsymbol{W}$ represents additive white Gaussian noise (AWGN) following $\mathrm{vec}(\boldsymbol{W}) \sim \mathcal{CN}(\boldsymbol{0}, N_0 \boldsymbol{I})$, with $\mathrm{vec}(\cdot)$ the vectorization operation, $\boldsymbol{0}$ the all-zeros vector and $\boldsymbol{I}$ the identity matrix. The goal of the sensing receiver is to detect the presence of the target and estimate its position based on $\boldsymbol{Y}$.

Observation with GPI: When the ULA elements are affected by GPIs, the actual steering vector of the ULA is $\boldsymbol{a}(\theta; \boldsymbol{\kappa}) = \boldsymbol{\kappa} \odot \boldsymbol{a}(\theta)$, where $\boldsymbol{\kappa} \in \mathbb{C}^N$ is a vector that contains the GPIs of all antenna elements. We consider that $\|\boldsymbol{\kappa}\|^2 = N$ so that under impairments the transmitter energy is preserved, i.e., $\|\boldsymbol{a}(\theta; \boldsymbol{\kappa})\|^2 = \|\boldsymbol{a}(\theta)\|^2 = N$. The model in (7) under GPIs becomes

$$\boldsymbol{Y} = t\gamma (\boldsymbol{a}(\theta; \boldsymbol{\kappa})(\boldsymbol{b}(\tau) \odot \boldsymbol{x})^{\top}) + \boldsymbol{W}. \tag{8}$$

The goal of the receiver is now to operate under unknown $\boldsymbol{\kappa}$.

[1]The communication receiver is not affected by GPI under the considered SIMO model. For this reason and due to space limitations, the communication performance is not evaluated in this paper.

III. Proposed Method

In the following, we detail the considered baseline to perform target detection and position estimation as well as the proposed unsupervised MB-ML approach to compensate for the GPIs.

A. Baseline

We assume that the baseline operates under a fixed $\boldsymbol{\kappa}$, which may not coincide with the true GPIs. In order to detect the target presence and estimate its position, we resort to the maximum a-posteriori ratio test (MAPRT) detector [32], which generalizes the generalized likelihood ratio test detector [33] to the case with random parameters and thus can take into account prior information on γ, θ and τ. We assume that the complex channel gain follows a normal distribution as $\gamma \sim \mathcal{CN}(0, \sigma_\gamma^2)$ and the target angle and range are confined to an a priori known region, i.e., $\theta \sim \mathcal{U}[\theta_{\min}, \theta_{\max}]$, $\tau \sim \mathcal{U}[\tau_{\min}, \tau_{\max}]$. Moreover, we assume that $p(t = 0) = p(t = 1) = 1/2$. For a fixed $\boldsymbol{\kappa}$, the MAPRT then yields the following optimal test:

$$\max_{\substack{\theta \in \mathcal{O} \\ \tau \in \mathcal{T}}} \big\{ |\boldsymbol{a}^{\mathsf{H}}(\theta; \boldsymbol{\kappa}) \boldsymbol{Y} (\boldsymbol{b}(\tau) \odot \boldsymbol{x})^*|^2 \big\} \gtrless \eta, \tag{9}$$

where $\mathcal{O} = [\theta_{\min}, \theta_{\max}]$, $\mathcal{T} = [\tau_{\min}, \tau_{\max}]$, $(\cdot)^{\mathsf{H}}$ denotes the conjugate transpose operation, $(\cdot)^*$ denotes the conjugate operation, $|\cdot|$ denotes the absolute value, and η is a threshold that controls the probabilities of detection and false alarm. Details about the derivation of the MAPRT can be found in Appendix A. The angle and delay of the target are obtained as follows:

$$(\hat{\theta}, \hat{\tau}) = \arg \max_{\substack{\theta \in \mathcal{O} \\ \tau \in \mathcal{T}}} \big\{ |\boldsymbol{a}^{\mathsf{H}}(\theta; \boldsymbol{\kappa}) \boldsymbol{Y} (\boldsymbol{b}(\tau) \odot \boldsymbol{x})^*|^2 \big\}. \tag{10}$$

When the assumed $\boldsymbol{\kappa}$ matches the actual GPIs, the baseline in (9), (10) is optimal and it represents a lower bound on the performance, as it will be shown in Sec. IV.

B. Proposed UL MB-ML Method

We base our approach on the baseline of Sec. III-A. In particular, we compute the *angle-delay* map as

$$\boldsymbol{M}(\hat{\boldsymbol{\kappa}}) = |\boldsymbol{\Phi}_\theta(\hat{\boldsymbol{\kappa}})^{\mathsf{H}} \boldsymbol{Y} (\boldsymbol{\Phi}_\tau \odot \boldsymbol{x} \boldsymbol{1}^{\top})^*|^2, \tag{11}$$

where $\hat{\boldsymbol{\kappa}}$ is the estimate of the GPIs, $\boldsymbol{1}$ is the all-ones vector, and

$$\boldsymbol{\Phi}_\theta(\hat{\boldsymbol{\kappa}}) = [\boldsymbol{a}(\theta_1; \hat{\boldsymbol{\kappa}})\ \boldsymbol{a}(\theta_2; \hat{\boldsymbol{\kappa}})\ \cdots\ \boldsymbol{a}(\theta_{N_\theta}; \hat{\boldsymbol{\kappa}})] \tag{12}$$

$$\boldsymbol{\Phi}_\tau = [\boldsymbol{b}(\tau_1)\ \boldsymbol{b}(\tau_2)\ \cdots\ \boldsymbol{b}(\tau_{N_\tau})]. \tag{13}$$

We evaluate the angle-delay map on a uniformly sampled 2D grid, with N_θ and N_τ the number of angle and delay points, respectively. From the angle-delay map, we propose two different unsupervised loss functions to learn the GPIs.

1) Maximize the maximum value of the angle-delay map:

$$\mathcal{J}(\hat{\boldsymbol{\kappa}}) = \mathbb{E}_{t, \gamma, \theta, \tau, \boldsymbol{x}, \boldsymbol{W}} \big[- \max_{i,j} [\boldsymbol{M}(\hat{\boldsymbol{\kappa}})]_{i,j} \big], \tag{14}$$

where the expectation is taken with respect to random realizations of $t, \gamma, \theta, \tau, \boldsymbol{x}$, and $\boldsymbol{W}$ in (8). Unknown GPIs reduce the magnitude of the angle-delay map, since computation of the angle-delay map involves $|\boldsymbol{a}^{\mathsf{H}}(\theta; \hat{\boldsymbol{\kappa}}) \boldsymbol{a}(\theta; \boldsymbol{\kappa})|^2$, which is only maximized if $\hat{\boldsymbol{\kappa}} = \boldsymbol{\kappa}$. Thus, we expect that by minimizing (14), our proposed algorithm converges to the true impairments $\boldsymbol{\kappa}$. Details about how the impairments affect the angle-delay map will be shown in Sec. IV.

Algorithm 1 Unsupervised MB-ML of the gain-phase errors.

Input: Initial GPIs $\boldsymbol{\kappa}^{(0)}$.
Output: Learned GPIs $\boldsymbol{\kappa}^{(I)}$.
for $i = 1, 2, \ldots, I$
  Draw a batch of realizations of: $t, \gamma, \theta, \tau, \boldsymbol{x}$, and $\boldsymbol{W}$.
  Compute $\boldsymbol{Y}$ according to (8).
  Construct $\boldsymbol{\Phi}_\theta(\boldsymbol{\kappa}^{(i)})$ and $\boldsymbol{\Phi}_\tau$ according to (12) and (13).
  Compute the angle-delay map following (11).
  Compute $\mathcal{J}(\boldsymbol{\kappa}^{(i)})$ according to (14) or (15).
  Update $\boldsymbol{\kappa}^{(i+1)}$ through gradient descent.
  Normalize $\boldsymbol{\kappa}^{(i+1)}$ so that $\|\boldsymbol{\kappa}^{(i+1)}\|^2 = N$.

2) Minimize the error of the received observation signal:

$$\mathcal{J}(\hat{\boldsymbol{\kappa}}) = \mathbb{E}_{t,\gamma,\theta,\tau,\boldsymbol{x},\boldsymbol{W}}\left[\|\boldsymbol{Y} - \widetilde{\boldsymbol{Y}}(\hat{\boldsymbol{\kappa}})\|_F\right], \tag{15}$$

where $\|\cdot\|_F$ denotes the Frobenius norm and

$$\widetilde{\boldsymbol{Y}}(\hat{\boldsymbol{\kappa}}) = \hat{\gamma}\boldsymbol{a}(\hat{\theta}; \hat{\boldsymbol{\kappa}})(\boldsymbol{b}(\hat{\tau}) \odot \boldsymbol{x})^\top \tag{16}$$

is the reconstructed observation from the channel gain, angle, and target delay estimations. The expression for $\hat{\gamma}$ is derived in Appendix A.[2] The motivation behind (15) is that the observation $\boldsymbol{Y}$ is affected by the true GPIs $\boldsymbol{\kappa}$, while we reconstruct the observation $\widetilde{\boldsymbol{Y}}$ in (16) using the estimated impairments $\hat{\boldsymbol{\kappa}}$. Our hypothesis is that by minimizing the difference between the received observation and the reconstructed signal, the learned impairments converge to the true impairments. Although the computation of $\hat{\theta}$ and $\hat{\tau}$ in (10) involves a nondifferentiable operation, it is possible to compute the gradient of the loss in (15) with respect to $\hat{\boldsymbol{\kappa}}$, which was already observed in an equivalent approach in [17].

In Algorithm 1, we summarize the proposed unsupervised MB-ML algorithm to learn the GPIs. The distributions of the random variables are highlighted in Table I. We initialize the algorithm with the ideal gain-phase coefficients, i.e., $\boldsymbol{\kappa}^{(0)} = \mathbf{1}$. Once we have learned the gain-phase errors according to Algorithm 1, we compute the same operations as the baseline in (9), (10) for inference, where the steering vector $\boldsymbol{a}^{\mathsf{H}}(\theta; \boldsymbol{\kappa})$ is replaced by the steering vector with the learned impairments $\boldsymbol{a}^{\mathsf{H}}(\theta; \boldsymbol{\kappa}^{(I)})$.

IV. Results

In this section, we detail the considered simulation parameters and present the sensing results[3] to assess the effectiveness of the proposed learning approach.

A. Simulation Parameters

In Table I the simulation parameters are outlined, where we consider that the communication symbols $[\boldsymbol{x}]_s$ are randomly drawn from a quadrature phase-shift keying (QPSK) constellation and $\measuredangle(\cdot)$ denotes the phase of a complex value. The SNR is $\text{SNR} = \mathbb{E}[\|\gamma(\boldsymbol{a}(\theta)(\boldsymbol{b}(\tau) \odot \boldsymbol{x})^\top)\|_F^2]/N_0 = \sigma_\gamma^2 NS/N_0$. The magnitude and phase of the GPIs are drawn from the distributions detailed in [36]. To evaluate the objective function to maximize in (9) and (10), we perform a uniformly 2D grid search over angles and delays, similarly to (11). During training, we leverage the Adam optimizer [37].

[2]The estimation of $\hat{\gamma}$ assumes knowledge of N_0/σ_γ^2, which is related to the signal-to-noise ratio (SNR). In this work we assume perfect knowledge of N_0/σ_γ^2, but we refer the reader to [34], [35] for SNR estimation methods.

[3]The code to reproduce all simulation results will be available in github.com/josemateosramos/UL_gain_phase_ISAC after the peer-review process.

TABLE I: Simulation parameters

Parameter	Expression	Value
N	-	64 antenna elements
f_c	-	60 GHz
d_{R}	$\lambda/2$	5 mm
S	-	256 subcarriers
Δ_{f}	-	240 kHz
T_{cp}	$0.07/\Delta_{\text{f}}$	-
t	$\mathcal{U}\{0, 1\}$	-
γ	$\mathcal{CN}(0, \sigma_\gamma^2)$	-
θ	$\mathcal{U}[\theta_{\min}, \theta_{\max}]$	-
$\theta_{\min}$	$\theta_{\text{mean}} - \Delta_\theta/2$	-
$\theta_{\max}$	$\theta_{\text{mean}} + \Delta_\theta/2$	-
θ_{mean}	$\mathcal{U}[-60°, 60°]$	-
Δ_θ	$\mathcal{U}[10°, 20°]$	-
τ	$\mathcal{U}[\tau_{\min}, \tau_{\max}]$	-
$\tau_{\min}$	$2R_{\min}/c$	$R_{\min} = 10$ m
$\tau_{\max}$	$2R_{\max}/c$	$R_{\max} = 43.75$ m
$\boldsymbol{x}$	$\mathbb{E}[\|\boldsymbol{x}\|^2] = S$	-
$\text{vec}(\boldsymbol{W})$	$\mathcal{CN}(\mathbf{0}, N_0\boldsymbol{I})$	-
SNR	$\sigma_\gamma^2 NS/N_0$	15 dB
$\lvert[\boldsymbol{\kappa}]_n\rvert$	$\mathcal{U}[0.95, 1.05]$	-
$\measuredangle([\boldsymbol{\kappa}]_n)$	$\mathcal{U}[-\pi/2, \pi/2]$	-
N_θ, N_τ	-	100
Learning rate	-	10^{-2}
Batch size	-	1024
Training iterations	-	10^4

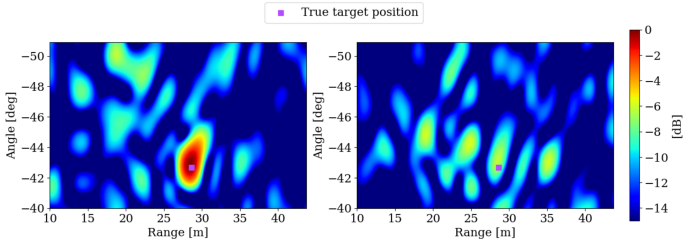

Fig. 2: Angle-delay map under full knowledge of the impairments (left) and assuming no impairments (right). The images are normalized with respect to the maximum of the angle-delay map under full knowledge of the impairments.

B. Impact of GPIs

To understand how ignoring the GPIs affects the sensing performance, we plot in Fig. 2 the angle-delay maps under full knowledge of the GPIs, i.e., $\hat{\boldsymbol{\kappa}} = \boldsymbol{\kappa}$ (left) and assuming no impairments, i.e., $\hat{\boldsymbol{\kappa}} = \mathbf{1}$ (right). The channel model in (8) includes an impairment realization $\boldsymbol{\kappa} \neq \mathbf{1}$. It is observed that disregarding GPIs changes the position of the maximum of the angle-delay map, which affects the test in (10). Furthermore, the angle-delay maps in Fig. 2 are normalized with respect to the maximum of the angle-delay map under full knowledge of GPIs (left), which implies that ignoring the GPIs also decreases the maximum magnitude of the angle-delay map compared to full knowledge of GPIs (as commented in Sec. III-B).

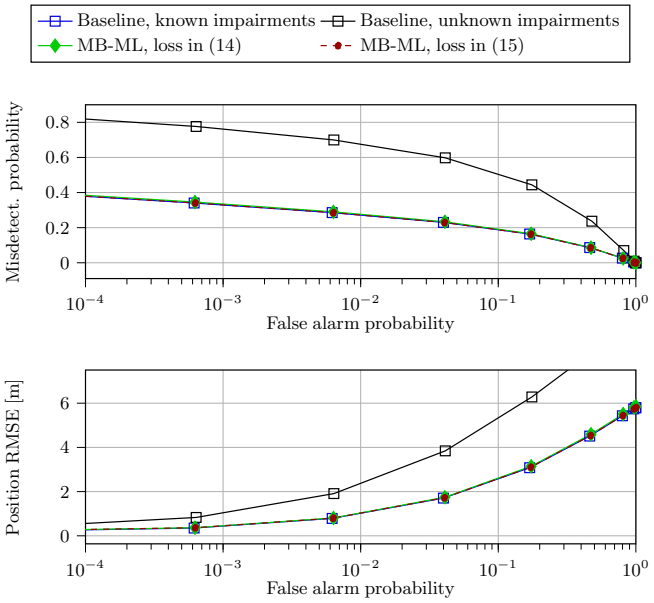

Fig. 3: Sensing results as a function of the false alarm probability.

C. Sensing Results

In Fig. 3, we show the testing sensing results, where we compare: (i) the baseline of Sec. III-A when $\boldsymbol{\kappa}$ matches the true impairments (in blue), (ii) the baseline with $\boldsymbol{\kappa} = \mathbf{1}$ (in black), and (iii) the proposed method of Sec. III-B with the learned impairments $\boldsymbol{\kappa} = \boldsymbol{\kappa}^{(I)}$, using the loss in (14) (in green) and the loss in (15) (in red). The results in Fig 3 are averaged over 100 realizations of the GPIs. The results in Fig. 3 indicate that the proposed unsupervised learning approach can converge to a GPI vector similar to the true impairments of the ULA and obtain similar performance as the case where the impairments are fully known. This confirms the hypothesis of Sec. III-B about the effectiveness of the proposed loss functions. Moreover, the performance of the algorithm using the losses (14) and (15) is very similar, which can be explained following the derivation of Appendix A. The loss in (15) resembles the objective to minimize in (20) and the loss in (14) is similar to (25). Both (20) and (25) are derived from the same MAPRT objective in (18). The results in Fig. 3 indicate that minimizing (14) or (15) is equivalent. The advantage of (14) is that is does not require knowledge of the SNR, while (15) can be more easily generalized to multiple targets and embedded in iterative algorithms like the orthogonal matching pursuit algorithm [38].

V. Conclusions

In this work, we have proposed a model-based unsupervised learning approach to account for GPIs in the RX ULA of an ISAC system. We have based our proposed approach on the optimal MAPRT, developing a differentiable approach that allows for backpropagation, and proposing two unsupervised loss functions that require no labeled data. Our results have shown that the proposed approach can effectively compensate for the effect of gain-phase errors in the RX ULA, yielding target detection and position estimation performances similar to the case where the impairments are fully known. Natural extensions include considering multiple targets and the GPI under a MIMO system.

Appendix A
Derivation of MAPRT

This appendix details the derivation of the MAPRT in Sec. III-A for single-target detection and position estimation. Since the target in the far-field is randomly present, we can formulate the target detection problem as a binary hypothesis testing problem:

$$\begin{aligned} \mathcal{H}_0 &: \boldsymbol{Y} = \boldsymbol{N} \\ \mathcal{H}_1 &: \boldsymbol{Y} = \gamma \boldsymbol{M}(\theta,\tau) + \boldsymbol{N}, \end{aligned} \tag{17}$$

where $\boldsymbol{M}(\theta,\tau) = \boldsymbol{a}(\theta;\boldsymbol{\kappa})(\boldsymbol{b}(\tau)\odot\boldsymbol{x})^\top$.

Note that the transmitted communication symbols $\boldsymbol{x}$ are known for the sensing receiver in the considered monostatic setup. Considering γ a random unknown, the MAPRT is

$$\mathcal{L}(\boldsymbol{Y}) = \frac{\max_{\gamma,\theta,\tau} p(\gamma,\theta,\tau,\mathcal{H}_1|\boldsymbol{Y})}{p(\mathcal{H}_0|\boldsymbol{Y})} \underset{\mathcal{H}_0}{\overset{\mathcal{H}_1}{\gtrless}} \eta. \tag{18}$$

Applying the Bayes' theorem to (18) yields

$$\mathcal{L}(\boldsymbol{Y}) = \frac{\max_{\gamma,\theta,\tau} p(\boldsymbol{Y}|\gamma,\theta,\tau,\mathcal{H}_1)p(\gamma)p(\theta)p(\tau)p(\mathcal{H}_1)}{p(\boldsymbol{Y}|\mathcal{H}_0)p(\mathcal{H}_0)} \underset{\mathcal{H}_0}{\overset{\mathcal{H}_1}{\gtrless}} \tilde{\eta}. \tag{19}$$

Assuming $p(\mathcal{H}_0) = p(\mathcal{H}_1) = 1/2$, $\gamma \sim \mathcal{CN}(0,\sigma_\gamma^2), \theta \sim \mathcal{U}([\theta_{\min},\theta_{\max}]), \tau \sim \mathcal{U}([\tau_{\min},\tau_{\max}])$ and taking the logarithm in (19), we obtain[4]

$$\mathcal{L}_{\log}(\boldsymbol{Y}) = \frac{\|\boldsymbol{Y}\|_F^2}{N_0} - \min_{\substack{\gamma \\ \theta\in\mathcal{O} \\ \tau\in\mathcal{T}}} \left\{ \frac{\|\boldsymbol{Y}-\gamma\boldsymbol{M}\|_F^2}{N_0} + \frac{|\gamma|^2}{\sigma_\gamma^2} \right\} \underset{\mathcal{H}_0}{\overset{\mathcal{H}_1}{\gtrless}} \bar{\eta}, \tag{20}$$

where $\mathcal{L}_{\log}(\boldsymbol{Y}) = \log(\mathcal{L}(\boldsymbol{Y}))$ and $\bar{\eta} = \tilde{\eta} + \log(\pi\sigma_\gamma^2) + \log(\theta_{\max}-\theta_{\min}) + \log(\tau_{\max}-\tau_{\min})$. The optimal γ for a given (θ,τ) in (20) is

$$\hat{\gamma} = \frac{\text{vec}(\boldsymbol{M})^{\mathsf{H}}\text{vec}(\boldsymbol{Y})}{\|\boldsymbol{M}\|_F^2 + N_0/\sigma_\gamma^2}. \tag{21}$$

Manipulating the expression in (20) and plugging (21) yields

$$\mathcal{L}_{\log}(\boldsymbol{Y}) = \max_{\substack{\theta\in\mathcal{O} \\ \tau\in\mathcal{T}}} \left\{ \frac{|\text{vec}(\boldsymbol{M})^{\mathsf{H}}\text{vec}(\boldsymbol{Y})|^2}{\|\boldsymbol{M}\|_F^2 + N_0/\sigma_\gamma^2} \right\} \underset{\mathcal{H}_0}{\overset{\mathcal{H}_1}{\gtrless}} \bar{\eta}. \tag{22}$$

Given the definition of $\boldsymbol{M}(\theta,\tau)$, we have that

$$\|\boldsymbol{M}\|_F^2 = N\|\boldsymbol{x}\|_2^2 \tag{23}$$

$$|\text{vec}(\boldsymbol{M})^{\mathsf{H}}\text{vec}(\boldsymbol{Y})|^2 = |\boldsymbol{a}^{\mathsf{H}}(\theta;\boldsymbol{\kappa})\boldsymbol{Y}(\boldsymbol{b}(\tau)\odot\boldsymbol{x})^*|^2. \tag{24}$$

Plugging (23) and (24) into (22) yields

$$\mathcal{L}_{\log}(\boldsymbol{Y}) = \max_{\substack{\theta\in\mathcal{O} \\ \tau\in\mathcal{T}}} \left\{ |\boldsymbol{a}^{\mathsf{H}}(\theta;\boldsymbol{\kappa})\boldsymbol{Y}(\boldsymbol{b}(\tau)\odot\boldsymbol{x})^*|^2 \right\} \underset{\mathcal{H}_0}{\overset{\mathcal{H}_1}{\gtrless}} \eta, \tag{25}$$

where $\eta = \bar{\eta}(N\|\boldsymbol{x}\|_2^2 + N_0/\sigma_\gamma^2)$. Once we have obtained the estimated $\hat{\theta},\hat{\tau}$, we can plug the estimations in (21).

References

[1] Y. Cui, F. Liu, C. Masouros, J. Xu, T. X. Han, and Y. C. Eldar, "Integrated sensing and communications: Background and applications," in *Integrated Sensing and Communications*. Springer, 2023, pp. 3–21.

[2] F. Liu, Y. Cui, C. Masouros, J. Xu, T. X. Han, Y. C. Eldar, and S. Buzzi, "Integrated sensing and communications: Towards dual-functional wireless networks for 6G and beyond," *IEEE J. Sel. Areas Commun.*, vol. 40, no. 6, pp. 1728–1767, Mar. 2022.

[4] We consider $\boldsymbol{M} \triangleq \boldsymbol{M}(\theta,\tau)$ for convenience.

[3] S. D. Liyanaarachchi, C. B. Barneto, T. Riihonen, M. Heino, and M. Valkama, "Joint multi-user communication and MIMO radar through full-duplex hybrid beamforming," in *Proc. 1st IEEE Int. Online Symp. Joint Commun. & Sens. (JC&S)*, Dresden, Germany, 2021, pp. 1–5.

[4] S. H. Dokhanchi, M. B. Shankar, M. Alaee-Kerahroodi, and B. Ottersten, "Adaptive waveform design for automotive joint radar-communication systems," *IEEE Trans. Veh. Technol.*, vol. 70, no. 5, pp. 4273–4290, Apr. 2021.

[5] M. F. Keskin, V. Koivunen, and H. Wymeersch, "Limited feedforward waveform design for OFDM dual-functional radar-communications," *IEEE Trans. Signal Process.*, vol. 69, pp. 2955–2970, Apr. 2021.

[6] L. Chen, F. Liu, W. Wang, and C. Masouros, "Joint radar-communication transmission: A generalized pareto optimization framework," *IEEE Trans. Signal Process.*, vol. 69, pp. 2752–2765, May 2021.

[7] J. Johnston, L. Venturino, E. Grossi, M. Lops, and X. Wang, "MIMO OFDM dual-function radar-communication under error rate and beampattern constraints," *IEEE J. Select. Areas Commun.*, vol. 40, no. 6, pp. 1951–1964, Mar. 2022.

[8] D. K. P. Tan, J. He, Y. Li, A. Bayesteh, Y. Chen, P. Zhu, and W. Tong, "Integrated sensing and communication in 6G: Motivations, use cases, requirements, challenges and future directions," in *Proc. 1st IEEE Int. Symp. Joint Commun. & Sens. (JC&S)*, Dresden, Germany, 2021, pp. 1–6.

[9] M. Alsabah, M. A. Naser, B. M. Mahmmod, S. H. Abdulhussain, M. R. Eissa, A. Al-Baidhani, N. K. Noordin, S. M. Sait, K. A. Al-Utaibi, and F. Hashim, "6G wireless communications networks: A comprehensive survey," *IEEE Access*, vol. 9, pp. 148 191–148 243, 2021.

[10] C. Liu, W. Yuan, S. Li, X. Liu, H. Li, D. W. K. Ng, and Y. Li, "Learning-based predictive beamforming for integrated sensing and communication in vehicular networks," *IEEE J. Sel. Areas Comm.*, vol. 40, no. 8, pp. 2317–2334, Jun. 2022.

[11] Y. Wu, F. Lemic, C. Han, and Z. Chen, "Sensing integrated DFT-spread OFDM waveform and deep learning-powered receiver design for terahertz integrated sensing and communication systems," *IEEE Trans. Commun.*, vol. 71, no. 1, pp. 595–610, Jan. 2023.

[12] Y. Liu, I. Al-Nahhal, O. A. Dobre, and F. Wang, "Deep-learning channel estimation for IRS-assisted integrated sensing and communication system," *IEEE Trans. Veh. Technology*, vol. 72, no. 5, pp. 6181–6193, May 2023.

[13] C. Muth, B. Geiger, D. G. Gaviria, and L. Schmalen, "Loss design for single-carrier joint communication and neural network-based sensing," in *Proc. 27th Int. Workshop on Smart Antennas (WSA)*, Dresden, Germany, 2024, pp. 131–137.

[14] N. Shlezinger, J. Whang, Y. C. Eldar, and A. G. Dimakis, "Model-based deep learning," *Proceedings of the IEEE*, vol. 111, no. 5, pp. 465–499, 2023.

[15] H. He, C.-K. Wen, S. Jin, and G. Y. Li, "Deep learning-based channel estimation for beamspace mmWave massive MIMO systems," *IEEE Wireless Commun. Lett.*, vol. 7, no. 5, pp. 852–855, Oct. 2018.

[16] X. Wei, C. Hu, and L. Dai, "Deep learning for beamspace channel estimation in millimeter-wave massive MIMO systems," *IEEE Trans. Commun.*, vol. 69, no. 1, pp. 182–193, Jan. 2021.

[17] T. Yassine and L. Le Magoarou, "mpNet: Variable depth unfolded neural network for massive MIMO channel estimation," *IEEE Transactions on Wireless Communications*, vol. 21, no. 7, pp. 5703–5714, July 2022.

[18] B. Chatelier, L. Le Magoarou, and G. Redieteab, "Efficient deep unfolding for SISO-OFDM channel estimation," in *ICC 2023 - IEEE International Conference on Communications*, 2023, pp. 3450–3455.

[19] P. Xiao, B. Liao, and N. Deligiannis, "DeepFPC: A deep unfolded network for sparse signal recovery from 1-bit measurements with application to DOA estimation," *Signal Process.*, vol. 176, p. 107699, Nov. 2020.

[20] L. Wu, Z. Liu, and J. Liao, "DOA estimation using an unfolded deep network in the presence of array imperfections," in *Proc. 7th IEEE Int. Conf. on Signal and Image Process. (ICSIP)*, Suzhou, China, 2022, pp. 182–187.

[21] D. H. Shmuel, J. P. Merkofer, G. Revach, R. J. van Sloun, and N. Shlezinger, "Subspacenet: Deep learning-aided subspace methods for DoA estimation," *arXiv preprint arXiv:2306.02271*, 2023.

[22] J. M. Mateos-Ramos, C. Häger, M. F. Keskin, L. L. Magoarou, and H. Wymeersch, "Model-based end-to-end learning for multi-target integrated sensing and communication," *arXiv preprint arXiv:2307.04111*, 2023.

[23] J. M. Mateos-Ramos, B. Chatelier, C. Häger, M. F. Keskin, L. Le Magoarou, and H. Wymeersch, "Semi-supervised end-to-end learning for integrated sensing and communications," in *Proc. 1st IEEE Int. Conf. Mach. Learn. Commun. Netw. (ICMLCN)*, Stockholm, Sweden, 2024, pp. 132–138.

[24] B. P. Ng, J. P. Lie, M. H. Er, and A. Feng, "A practical simple geometry and gain/phase calibration technique for antenna array processing," *IEEE Trans. Antennas Propag.*, vol. 57, no. 7, pp. 1963–1972, 2009.

[25] C. Liu, X. Tang, and Z. Zhang, "A new gain-phase error pre-calibration method for uniform linear arrays," *Sensors*, vol. 23, no. 5, p. 2544, 2023.

[26] Y. Li, K. Lee, and Y. Bresler, "Blind gain and phase calibration via sparse spectral methods," *IEEE Trans. Inf. Theory*, vol. 65, no. 5, pp. 3097–3123, 2019.

[27] X. Jie, B. Zheng, and B. Gu, "Gain and phase calibration of uniform rectangular arrays based on convex optimization and neural networks," *Electronics*, vol. 11, no. 5, p. 718, 2022.

[28] Z. Zhou, Z. Wei, J. Ren, Y. Yin, G. F. Pedersen, and M. Shen, "Transfer-learning-assisted multielement calibration for active phased antenna arrays," *IEEE Trans. Antennas Propag.*, vol. 71, no. 2, pp. 1982–1987, 2023.

[29] L. Pucci, E. Paolini, and A. Giorgetti, "System-level analysis of joint sensing and communication based on 5G new radio," *IEEE J. Select. Areas Commun.*, vol. 40, no. 7, pp. 2043–2055, Mar. 2022.

[30] J. B. Sanson, P. M. Tomé, D. Castanheira, A. Gameiro, and P. P. Monteiro, "High-resolution delay-doppler estimation using received communication signals for OFDM radar-communication system," *IEEE Trans. Veh. Technology*, vol. 69, no. 11, pp. 13 112–13 123, Sep. 2020.

[31] M. F. Keskin, H. Wymeersch, and V. Koivunen, "MIMO-OFDM joint radar-communications: Is ICI friend or foe?" *IEEE J. of Select. Topics Signal Process.*, vol. 15, no. 6, pp. 1393–1408, Sep. 2021.

[32] S. Guruacharya, B. K. Chalise, and B. Himed, "MAP ratio test detector for radar system," *IEEE Trans. Signal Process.*, vol. 69, pp. 573–588, Dec. 2021.

[33] E. Conte, A. De Maio, and G. Ricci, "GLRT-based adaptive detection algorithms for range-spread targets," *IEEE Trans. Signal Process.*, vol. 49, no. 7, pp. 1336–1348, Jul. 2001.

[34] D. Pauluzzi and N. Beaulieu, "A comparison of snr estimation techniques for the awgn channel," *IEEE Trans. Commun.*, vol. 48, no. 10, pp. 1681–1691, 2000.

[35] A. Wiesel, J. Goldberg, and H. Messer-Yaron, "SNR estimation in time-varying fading channels," *IEEE Trans. Commun.*, vol. 54, no. 5, pp. 841–848, 2006.

[36] J. Jiang, F. Duan, J. Chen, Z. Chao, Z. Chang, and X. Hua, "Two new estimation algorithms for sensor gain and phase errors based on different data models," *IEEE Sensors J.*, vol. 13, no. 5, pp. 1921–1930, 2013.

[37] D. P. Kingma and J. Ba, "Adam: A method for stochastic optimization," in *Proc. 3rd Int. Conf. Learn. Representations (ICLR)*, San Diego, CA, USA, 2015.

[38] J. Lee, G.-T. Gil, and Y. H. Lee, "Channel estimation via orthogonal matching pursuit for hybrid MIMO systems in millimeter wave communications," *IEEE Trans. Commun.*, vol. 64, no. 6, pp. 2370–2386, Apr. 2016.